INL/EXT-08-15161

PIV Experiments to Measure Flow Phenomena in a Scaled Model of a VHTR Lower Plenum

Hugh M. McIlroy, Jr.
Donald M. McEligot
Richard R. Schultz
Daniel Christensen
Robert J. Pink
Ryan C. Johnson

September 2006

The INL is a U.S. Department of Energy National Laboratory
operated by Battelle Energy Alliance

INL/EXT-08-15161

PIV Experiments to Measure Flow Phenomena in a Scaled Model of a VHTR Lower Plenum

Hugh M. McIlroy, Jr.
Donald M. McEligot
Richard R. Schultz
Daniel Christensen
Robert J. Pink
Ryan C. Johnson

September 2006

Idaho National Laboratory
Idaho Falls, Idaho 83415

http://www.inl.gov

Prepared for the
U.S. Department of Energy
Office of Nuclear Energy
Under DOE Idaho Operations Office
Contract DE-AC07-05ID14517

Abstract

A report of experimental data collected at the Matched-Index-of-Refraction (MIR) Laboratory in support of contract DE-AC07-05ID14517 and the INL Standard Problem on measurements of flow phenomena occurring in a lower plenum of a typical prismatic VHTR concept reactor to assess CFD code is presented. Background on the experimental setup and procedures is provided along with several samples of data obtained from the 3-D PIV system and an assessment of experimental uncertainty is provided. Data collected in this study include 3-dimensional velocity-field descriptions of the flow in all four inlet jets and the entire lower plenum with inlet jet Reynolds numbers (Re_{Jet}) of approximately 4300 and 12,400. These investigations have generated over 2 terabytes of data that has been processed to describe the various velocity components in formats suitable for external release and archived on removable hard disks. The processed data from both experimental studies are available in multi-column text format.

Table of Contents

Table of Contents iii

Nomenclature iv

Introduction 1

Background 1

Formulation of a Standard Problem 1

Summary of Previous Work 4

Experimental Setup 5

Matched-Index-of-Refraction (MIR) Facility 5

Particle Image Velocimetry (PIV) System 6

Experimental Model 7

Experimental Procedures 9

MIR Primary Flow Loop 9

PIV System 10

Data Processing 11

Experimental Results 12

Re_{Jet} 4300 12

Inlet Jets 13

Lower Plenum 14

Re_{Jet} 12400 17

Uncertainty Analysis 17

Estimates of PIV Measuring Uncertainties 18

Sample Size 19

Positioning Uncertainties 20
Seeding Particle Settling Velocity 21
Fluid Properties 21
Geometry 22
Flow Rates 22
Reynolds Numbers 24
Summary and Conclusions 24
Recommendations for Further Study 25
Endnotes 26

Nomenclature

a	Particle radius
dt	Time separation between double frames of one camera
D, d	Diameter
D_h	Hydraulic diameter, $D_h = \frac{4 \cdot A_{CS}}{P_w}$
g	Acceleration of gravity
$\dot{m}$	Mass flow rate
N	Number of independent realizations
Q	Volume flow rate
RMS, rms	Root mean square
t	Time
T	Temperature
Unc	Uncertainty
V	Mean velocity component
V_b	Bulk or mixed-mean streamwise velocity, G/ρ
x	Streamwise coordinate
y	Wall-normal coordinate
z	Spanwise coordinate

Non-dimensional quantities

Re	Reynolds number, $\mathrm{Re} = \frac{4 \cdot \dot{m}}{\pi D \mu}$
Re_{Dh},	Re based on hydraulic diameter, $\mathrm{Re} = \frac{G \cdot D_H}{\mu}$

Greek symbols

δ	Uncertainty of ___
μ	Absolute viscosity
ν	Kinematic viscosity, $\upsilon = \frac{\mu}{\upsilon}$
ρ	Density
σ	Uncertainty of (quantity indicated by subscript)

Subscripts

b	Evaluated at bulk or mixed-mean temperature

D	Based on diameter
Dh	Evaluated with hydraulic diameter
f	Fluid
i	Evaluated at inlet, entry
j, Jet	Jet
p	Particle
pix	Pixel

INTRODUCTION

Background

The Very High Temperature Reactor (VHTR) is the most likely candidate for the Next Generation Nuclear Plant (NGNP). Because of the high temperatures characteristic of the VHTR, it is important to be able to simulate the turbulent flow in the reactor, especially in the lower plenum where the coolant is hottest, in order to ensure that large temperature gradients are not present in the coolant that could adversely impact structural materials. It is recognized that to simulate the flow in the VHTR lower plenum, advanced computational fluid dynamic (CFD) codes using appropriate turbulence modeling will be necessary.

Formulation of a Standard Problem

A challenge of designing and licensing the VHTR is to confirm that the intended analysis tools can be used confidently to make decisions and to assure that the reactor systems are safe and meet the performance objectives of the Generation IV Program. The research and development (R&D) projects defined in the VHTR Methods Program will ensure that the tools used to perform the required calculations and analyses can be trusted. The Methods R&D tasks are designed to ensure that the calculational envelope of the tools used to analyze the VHTR reactor systems encompasses, or is larger than, the operational and transient envelope of the VHTR itself.

Computational fluid dynamics (CFD) analyses will be a major component in the analysis suite that will be required to design and license the VHTR so the reactor can operate at maximum outlet temperatures and efficiencies. Only CFD analysis tools have the capability to determine where localized hot spots will occur in the reactor and also whether or not unacceptably large thermal gradients are present. Consequently, the major objectives of the VHTR Methods Program are to: develop the methodologies to be used for validating the CFD tools, gain acceptance from the community and the licensing authorities for the correct application of CFD to VHTR problems, and to develop practices and procedures that minimize the user effect, determine the requirements for building and accepting validation experimental data sets, enable the numerical uncertainty to be quantified, and standardize the efforts for performing needed CFD calculations.

The calculational envelope of the CFD tools used to analyze the behavior of the VHTR is defined by the scenarios and phenomena that these tools can calculate with confidence. CFD tools can only be used confidently when the results they produce have been shown to be in reasonable agreement with first-principle results, thought-problems, and data that describe the "highly ranked" phenomena inherent in all operational conditions and important accident scenarios for the VHTR. Reasonable agreement is achieved when the calculation generally lies within the uncertainty band of the data used for validation and always shows the same trends as the data and when code deficiencies are minor

The R&D process itself is outlined in Figure 1. The requirements associated with scenario identification, defining the phenomena identification and ranking tables (PIRT), completing the required development, and performing the necessary validation studies must all be completed prior to performing the required analyses confidently.

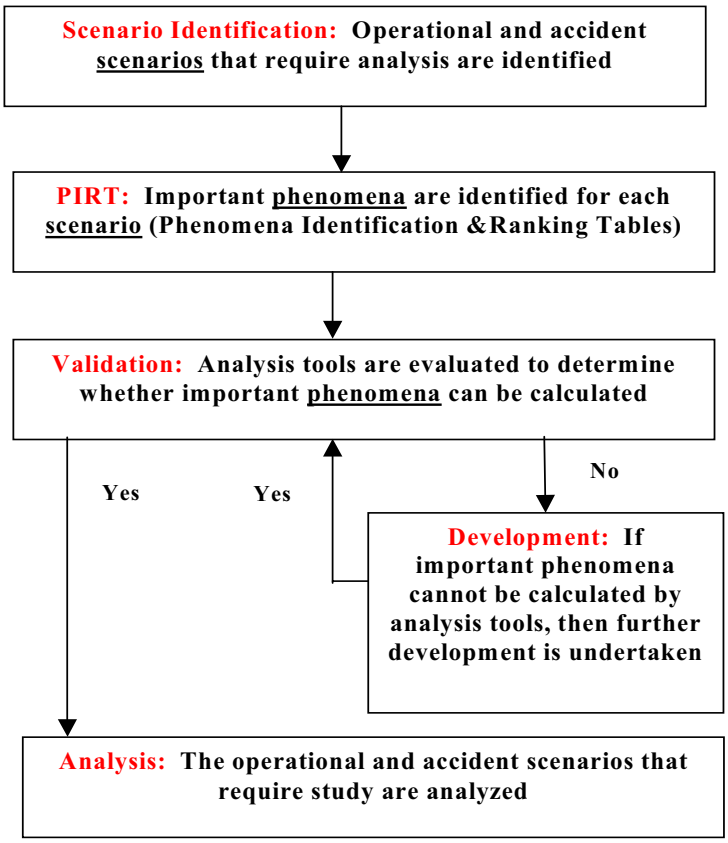

Figure 1. Research and development process.

Presently, the CFD tools to be used for analyzing the VHTR are not ready to perform design and analysis, nor are they ready for licensing calculations to the standard that will be required by the VHTR. Considerable validation, and perhaps development of the software tools, are required. Additionally, practices and procedures are required for both validating and developing the necessary CFD software that are acceptable to the nuclear community.

These conclusions follow since the key phenomena for the most challenging scenarios that must be analyzed for the to-be-selected VHTR have not been identified yet, software tools that have a low calculational uncertainty will be required to analyze the behavior of the VHTR to enable the plant to operate at a high efficiency with a competitive economic margin, and most of the software tools that will be used have not been validated for the scenarios and phenomena that must be analyzed. For example, although CFD software has been validated for selected cases, a full validation has not been performed nor are the data available that will enable a full validation to be performed. Finally, CFD analyses, which will be widely used to analyze the VHTR behavior, have never been used in large measure to perform auditing, design, or licensing calculations for a nuclear plant.

The validation process is based on developing a set of standard problems that will populate a validation matrix for the various tools. The structure in place for performing standard problems is shown in Figure 2.

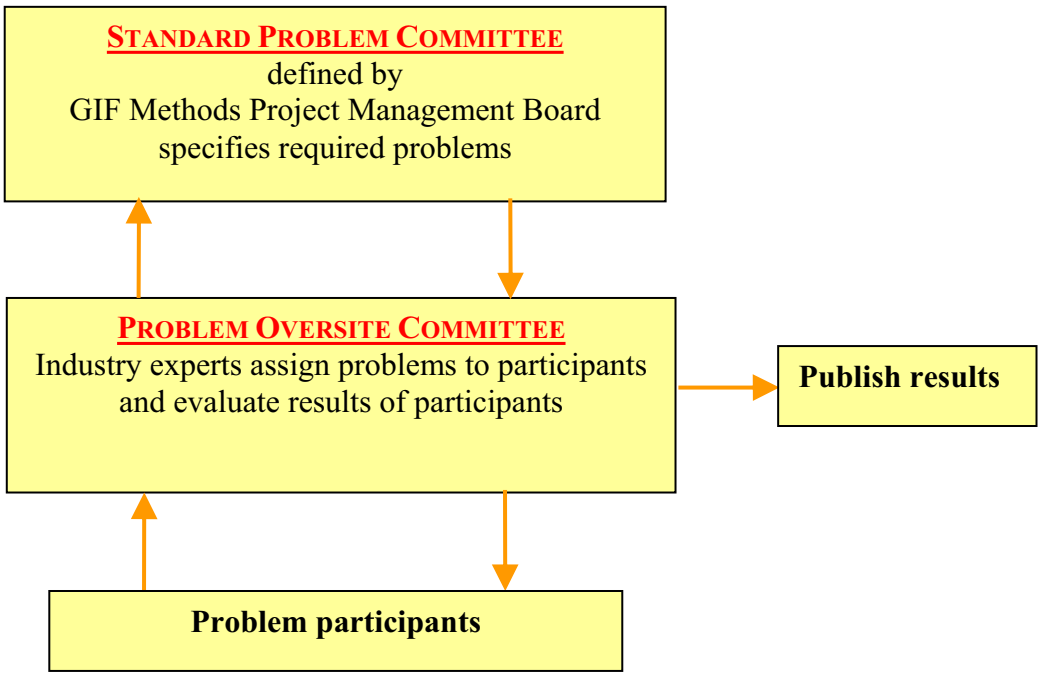

Figure 2. Process for specifying standard problems and implementing standard problem exercises.

The standard problems are defined by the Generation IV International Forum (GIF) Standard Problem Committee which defines its standard problems on the basis of comprehensive phenomena identification and ranking tables (PIRT)[1]. The standard problems, which are defined using high-quality data sets with known uncertainty bands, are the measure used to determine whether or not an analysis tool is capable of calculating the required phenomena. The members of the Standard Problem Committee are experts in the potential scenarios that are projected to be important in the VHTR.

The standard problems are passed to the Problem Oversight Committee. Members of this committee are experts in using and validating the analysis tools. Some members of this committee were specifically chosen due to their expertise in other industries where CFD is widely used. This committee defines the practices and procedures that must be used to perform the standard problems and they also distribute the standard problem to the participants. Finally, the Problem Oversight Committee is responsible for coordinating the comparisons between the participant's solutions and the experimental results including the evaluation of the validation. It is understood that many of the standard problem's calculations will be "blind," that is the participants will not be privy to the experimental data while their calculation is in progress.

Standard problems form the basis for determining whether a software tool is capable of analyzing the behavior of a reactor system undergoing a review for an operating license. The term "standard problem" stems from the use of the data sets that make up these problems as a measure (hence, a standard) to determine the acceptability of the software.

Standard problems consist of data sets that have the following characteristics:

a. The data set describes a phenomenon, or a set of phenomenon, that influences the behavior of an important figure-of-merit. That is, given the figure-of-merit is the reactor vessel wall temperature and the reactor vessel wall temperature must be less than a predetermined value, then important phenomena influence the reactor vessel wall temperature. Such phenomenon is identified in phenomena identification and ranking studies (see flow chart shown in Figure 1) and are documented (Lee, Wei, and Schultz 2005). An example of such a phenomenon is turbulent mixing of hot exit gases in the reactor vessel lower plenum since hot jets with an above average temperature may impinge on the outlet plenum wall and perhaps cause a local hot spot on the reactor vessel wall.

b. The phenomenon given in the standard problem data set, although it may be measured in a reduced-scale system, can be scaled to the full-sized system using accepted scaling practices. The scaling studies that link the experimental apparatus and data to the full-sized system are documented in a report.

c. The standard problem data set has been shown to measure the data required to determine whether the software are capable of calculating the important phenomenon.

d. The standard problem data set has uncertainties associated with each data point.

e. The quality assurance (QA) procedures used to design the experiment, build the experiment, and conduct the experiment are consistent with NQA-1 requirements.

The data summarized in this report are to validate CFD software and the MIR experiment meets the above requirements as described in this report.

Summary of Previous Work

The scaling, design, fabrication and installation of the first experiment to validate the computational tools (CFD codes) and the standard problem software have been completed and previously reported [2]. McEligot and McCreery [3] documented scaling studies and conceptual designs for flow and heat transfer experiments intended to assess CFD codes and their turbulence models proposed for application to prismatic VHTR concepts. Condie et al. [4] documented the design of a first experiment to measure generic flow phenomena expected to occur in the lower plenum of a typical prismatic VHTR. The product of these efforts resulted in the fabrication and installation of a scaled model of the region of a typical VHTR lower plenum that is near the outer reflector wall away from the plenum outlet.

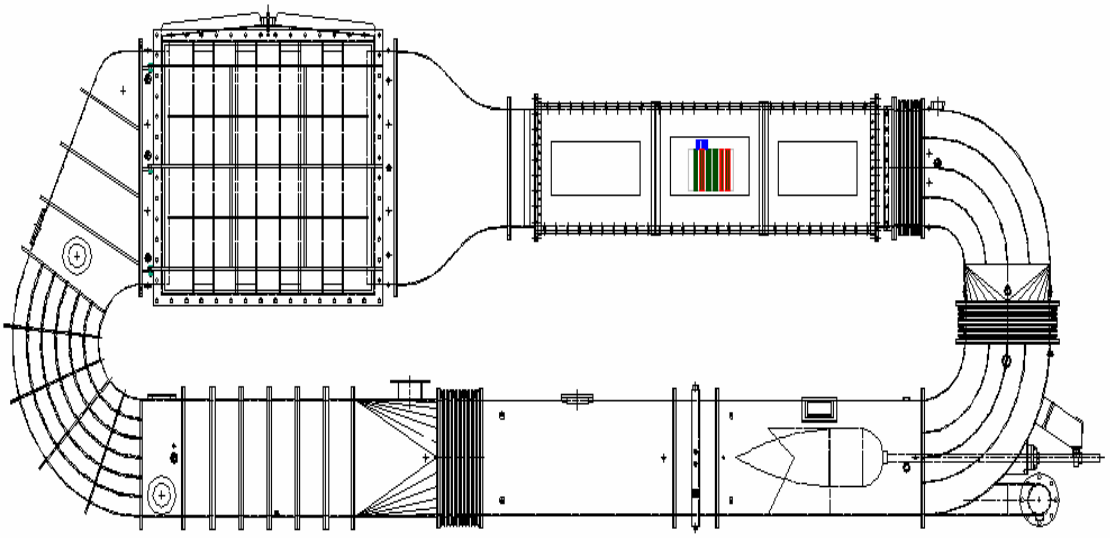

The working fluid for this experiment is light mineral oil, The working fluid is circulated around the loop (clockwise in Figure 3) by a 75-hp variable speed axial pump that can provide a maximum volumetric flow rate of approximately 0.6 m^3/sec of mineral oil. This maximum volumetric flow rate corresponds to a maximum inlet velocity to the test section of approximately 1.7 m/sec. The test section includes three chambers that are constructed of 3.8 cm thick polycarbonate supported by a stainless steel framework. Each chamber is fined with a removable lid. The test section inside dimension is 0.61m square and it is 2.44 m long. Each chamber of the test section is equipped with glass window inserts in the side panels to accommodate high quality measurements with laser Doppler velocimetry (LDV) and/or particle image velocimetry (PIV). The entire facility is supported on pneumatic vibration isolators.

The working fluid temperature is maintained with an auxiliary temperature control loop as shown in Figure 4. This loop extracts approximately 300 L/min of mineral oil from the primary flow loop through two pipes just upstream of the main circulation pump. The fluid is pumped through a glycol-cooled heat exchanger and a 10kW DC heater for temperature control and through an in-line filter to remove particulates greater than 5 μm in diameter. The fluid is then re-injected into the primary flow loop downstream of the main circulation pump through 3 orifices that are 3mm in diameter evenly spaced on a peripheral ring attached to the main flow channel. This temperature control system can maintain the fluid temperature in the test section to

within ± 0.05 ^{0}C of the specified temperature. An additional auxiliary flow loop, with the same temperature control mechanism, is used to provide fluid for the inlet jets of the VHTR lower plenum model. As shown in Figure 4 fluid is extracted from the primary flow loop and routed to a seven horsepower auxiliary pump that produces high-pressure, high speed flow to the model inlet jets. To maintain the required working fluid temperature, a portion of this fluid is extracted from the primary loop and routed through a parallel secondary temperature control loop. As in the primary temperature control loop the mineral oil is cooled and reheated then returned to the auxiliary flow loop and into the model inlet jets. The facility includes instrumentation to control the flow and to conduct measurements. Control instrumentation includes thermistor probes, thermistors, flow meters, data acquisition and computer controls.

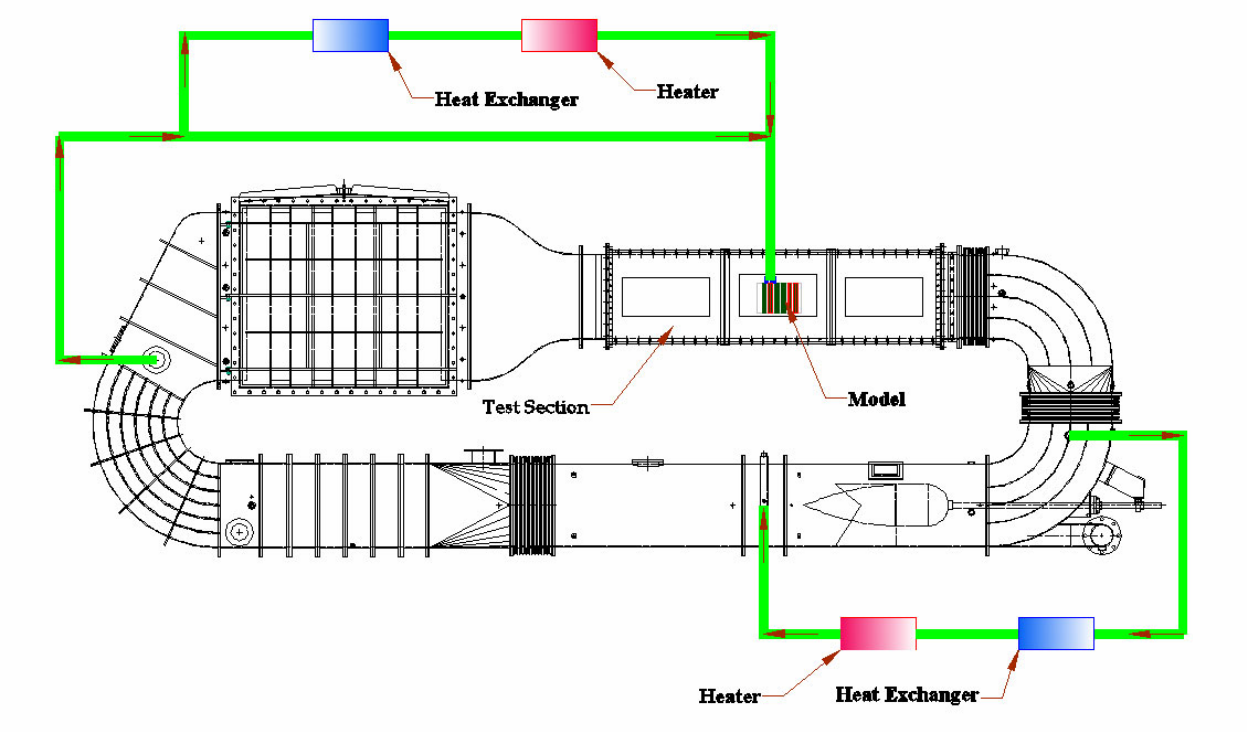

Figure 4. MIR Facility Temperature Control System.

Particle Image Velocimetry (PIV) System

Velocity field measurements were obtained with a 3-D PIV from LaVision, Inc. The 3-D PIV system consists of two ImagePro Plus digital CCD cameras and a double-pulsed Nd:YAG laser from Big Sky Laser. The system is controlled with DaVis 7.1 software in a LaVision dual-processor Programmable Timing Unit (PTU). The PIV system cameras are mounted on a 3-dimensional traverse system that is controlled by three separate electric stepping motors. The cameras can be positioned and re-positioned to with 2 micron accuracy using linear stages and digital readouts at the operator's station. The laser is also controlled with an electric stepping motor. The laser can be positioned and re-positioned to within *5* micron accuracy with an optical linear stage and digital readout that is also located at the operator's station. A two-component, TSI fiberoptic-based laser Doppler velocimeter is also available for velocity field measurements.

Experimental Model

Figure 5 is a picture of the experimental model that was installed in the test section of the MIR Facility. The model is fabricated from fused quartz and carefully fixed in the MIR Flow

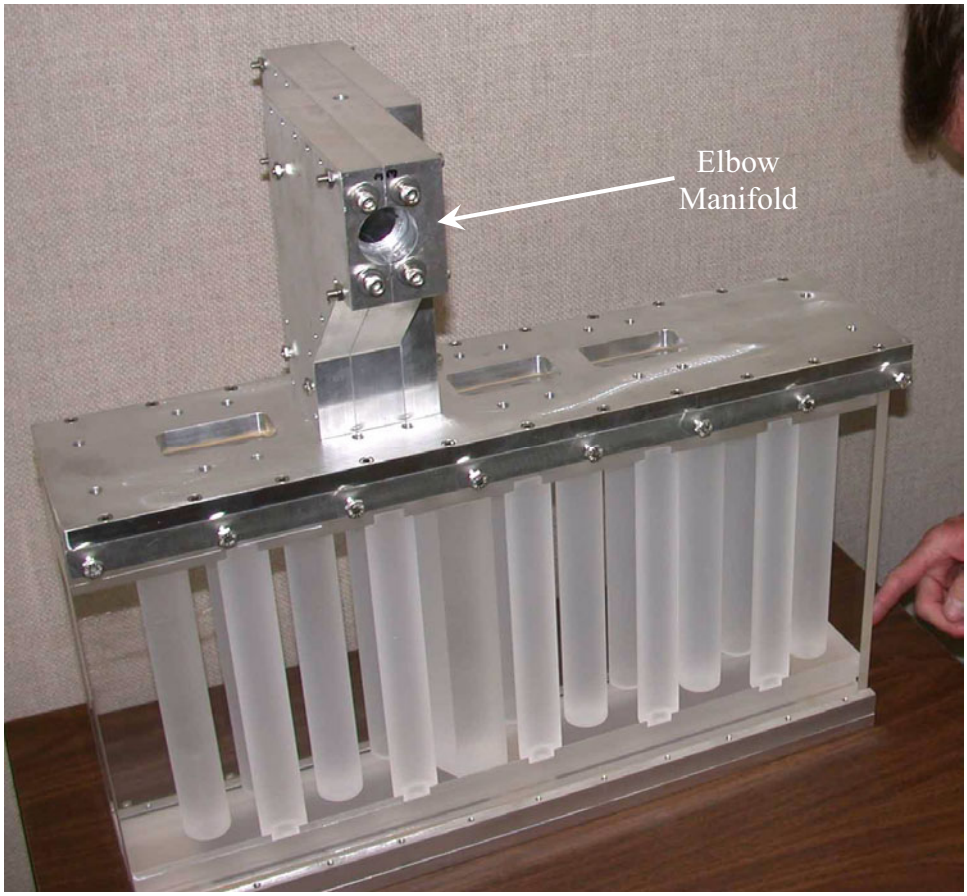

Figure 5. Quartz Experimental Model.

Facility Test Section (see Appendix A of Condi et al. [2005] for detailed drawings of the model). Mineral oil in the Primary Flow Loop flows around the model in the (clockwise direction in Figure 4) for temperature control of the external surfaces of the model. Mineral oil from the Auxiliary Loop flows into the model jets on the top of the model via four inlet jet elbow manifolds. The four inlet jet flows merge in the lower plenum and flow toward the outlet end of the model where the flow exits and merges with the primary loop flow. The four jet inlet flows are conditioned in the elbow manifolds to meet conditions expected to be present in the actual VLITR cooling channels. When the inlet jet flows reach the upper portion of the model the flows are turned by a machined elbow manifold (shown on the top of the model in Figure 5) where it is straightened. The inlet jet flow then passes over a turbulence generator to induce expected levels of turbulence. Key requirements for the inlet jet flow are that the flow turbulent, uniform and contains negligible swirl.

Figure 6 is a picture of the experimental model installed in the MIR Flow facility test

section and the PIV system setup. Note the location of the laser head beneath the test section.

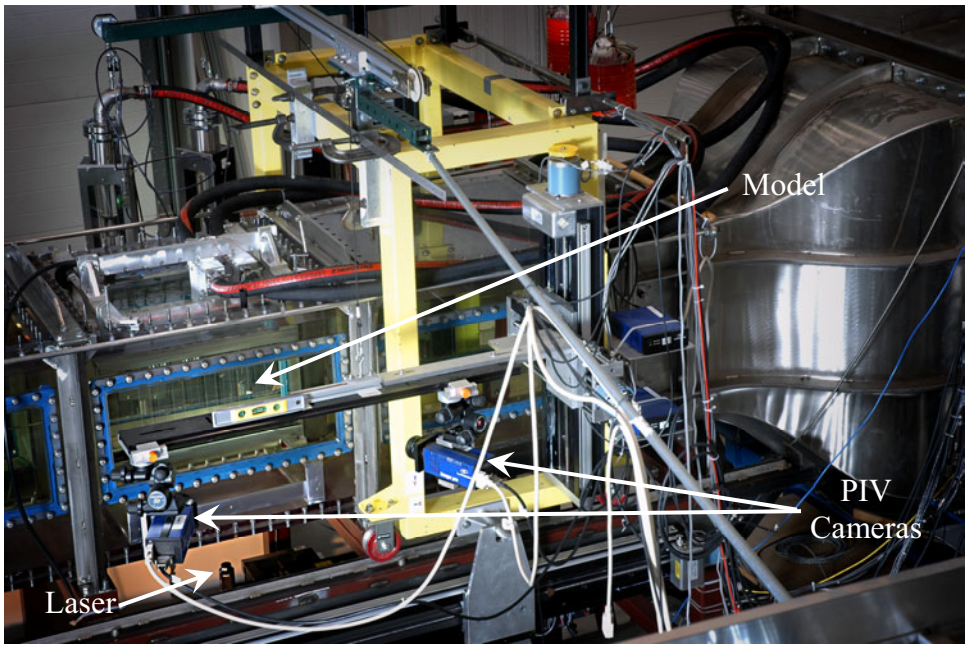

Figure 6. MIR Test Section, Experimental Model and PIV System.

Figure 7 is a close up view of the MIR Test Section and the quartz model. The four inlet jets are visible in the upper right corner of the model along with four aluminum plugs installed in

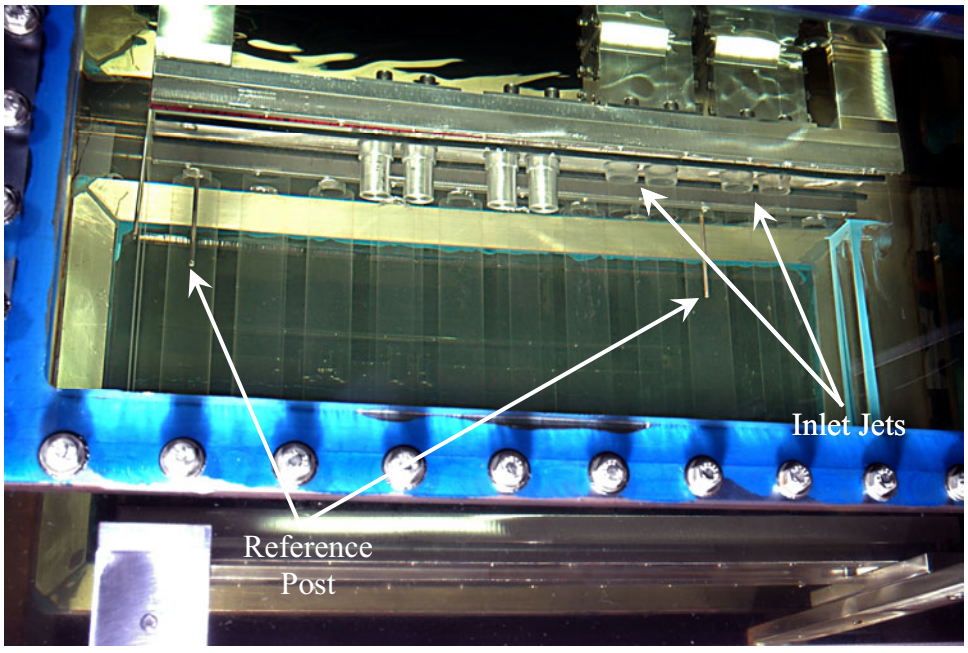

Figure 7. Close-up of MIR Test Section and Experimental Model

jets 5- 8 in the upper center of the model. Additionally, two reference posts are visible. These

reference posts are used to scale the PIV software coordinate system to the model coordinate system.

Figure 8 is a picture of the four large flow meters that are used to control the flow rates of each inlet jet. Flow enters the flow meters from the large cylindrical manifold below the manifolds which is fed by the Auxiliary Flow loop. The flow is controlled by large gate valves attached to the manifold below the flow meters. Flow passes through the flow meters and travels to the inlet jets via large tubes that connect the flow meters and the inlet conditioning manifolds.

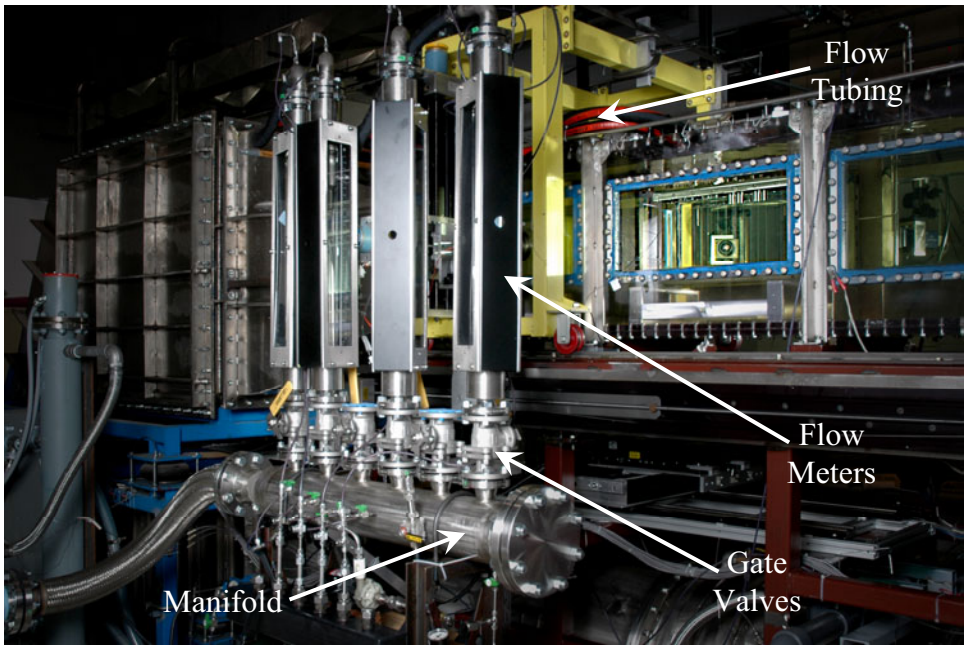

Figure 8. Inlet Jet Control System.

EXPERIMENTAL PROCEDURES

MIR Primary Flow Loop

Mineral oil that is normally stored in 8 large 1,000 gallon stainless steel tanks on the mezzanine floor in the MIR Lab was transferred to the MW. flow system at the beginning of this effort. The initial charge of mineral oil was left in the flow facility for the duration of the experiment. This practice maintained the mineral oil, and several charges of seeding particles that were added over time, to remain in the flow facility and limited the requirements for re-seeding.

The first step in the standard experimental procedure was to energize the Main Oil Loop Circulating Pump. This pump was operated at 75 rpm to circulate the mineral oil through the main oil loop and test section for temperature control. As soon as the mineral oil in the main oil loop reached a steady, constant velocity, the Auxiliary Flow Loop and Auxiliary Temperature

Control Loop were engaged. The Auxiliary Flow Control Pump was set to a pre-determined setting so that the required flow through the four flow meters feeding each of the inlet jets could achieve the required flow rate. When the main loop oil temperature reached approximately 22^0C the glycol chiller, located outside the MIR Lab, was engaged. The temperature of the Main Loop and Auxiliary Flow Loop was controlled with Lab VIEW software. Once the system reaches the predetermined set point the temperature control system maintains the oil temperature to within + 0.05 ^{0}C in the model and to within ± 0.03 ^{0}C in the main loop. The facility remains at a constant, steady state condition throughout the data collection period Temperature records for all data collection files are archived on the Temperature Control PC.

PIV System

Once the Main Flow Loop had reached steady state, the PIV system was energized. This system does not require a warm-up period so it is available for service as soon as it is energized. The PIV system was operated in the 3-D, Expert User mode. The PIV Camera Carriage (that supported both digital cameras) was positioned at the location were measurements would be taken. Laser power, Q-Switch delays and the time between frames of the double-image cameras (dt) were adjusted using the DaVis software Interactive Mode.

The cameras were mounted on a long cantilever bar from the vertical stage of the camera traverse system. This technique was necessary in order to arrange the cameras for 3-D measurements. The cantilevered bar and cameras caused severe strain on the vertical stage stepping motor so a camera counter-balance system was installed on the top of the camera traverse carriage. This system effectively neutralized the problem of strain on the vertical stage stepping motor.

In an effort to balance the requirement for high resolution data and vector fields along with the requirement to keep the size of data files within reasonable limits (for data processing and data storage considerations) the collection effort on the model was divided into 8 regions. The lower plenum area of the model was divided into six regions and each pair of inlet jets (jets l&2 and jets 3&4) were investigated as a single region. Additionally, in order to collect spanwise (3-D) data across the entire span of the model the laser and cameras were positioned at 23 light different spanwise planes. The laser light sheet was adjusted to a thickness of about 2 mm which allowed for complete, continuous coverage of the model – except the area near the walls of the model where the laser light sheet was blocked by 0-rings seals.

Because of the refractive index difference between the air space where the cameras operated and the mineral oil where the light sheet was located, it was necessary to coordinate the movement of the two digital cameras relative to the movement of the laser light sheet. This coordination was accomplished with a MATHCAD code. The code used the mineral oil temperature to determine the index of refraction of the mineral oil along with the camera angles relative to the laser light sheet reported by the camera calibration procedure. By inputting the camera angles the code produced a movement ratio (y_{Camera}/y_{Laser}) of the camera distance to the laser light sheet distance. This ratio was typically between 0.62 and 0.68

Table 1 summarizes the settings used on the MIR Flow facility and 3-D PIV system for data collection in the Re_{Jet} 4300 experiments and the present Re_{Jet} 12400 experiments.

MIR Loop Component	Setting	
Main Circulation Pump (dial/readout in rpm)	131/75	
Auxiliary Loop Pump (dial – Hz)	65	
Auxiliary Loop Temperature Control Pump (dial)	7.0	
Chiller Set Point (readout - ºC)	18.5	
Glycol Pump (dial)	5.5	
Glycol Flow to Primary Temperature Control Loop (gpm)	25.5	
Glycol Flow to Auxiliary Temperature Control Loop (gpm)	14	
	Re_{Jet} 4300	Re_{Jet} 12400
Auxiliary Loop Temperature Control Pump (L/min)	27.0	74.8
Auxiliary Loop Flow (LabVIEW input – L/min)	205.48	593.37
Jet No. 1 Flow Rate (gpm)	11.25	32.11
Jet No. 2 Flow Rate (gpm)	16.75	48.14
Jet No. 3 Flow Rate (gpm)	16.75	48.14
Jet No. 4 Flow Rate (gpm)	16.75	48.14
PIV System		
Camera Mode	3-D Cross Correlation	3-D Cross Correlation
Trigger	Internal	Internal
Trigger Delay (μs)	4	4
dt	Various	Various
Laser Power	Various	Various
Q-Switch Delays @ Maximum Power (Laser 1/Laser 2)	175/175	Various
Q-Switch Delays @ Minimum Power (Laser 1/Laser 2)	370/385	Various
Image Acquisition Method	RAM (fast)	Standard
Camera Binning	Off	Off
Acquisition – Number of Images	170	750

Table 1. MIR and PIV Settings.

Data Processing

Post-processing of data from the Re_{Jet} 4300 experiments was accomplished with DaVis 7.1 software. The post-processed data was then exported from DaVis to a secondary PC where data was organized and displayed with TecPlot.

EXPERIMENTAL RESULTS

Re_{Jet} 4300

Figure 9 is a snapshot of a flow visualization movie clip of flow in the lower plenum model with all four jets operating at Re_{Jet} 4300 (based on jet diameter and bulk flow velocity). The video clip was obtained by injecting air into the flow of jet 1. Air was not injected into all four jets because the resulting mass of air bubbles made visualization of the flow structure impossible. The movie clip provided a general reference for the flow field and was a reality

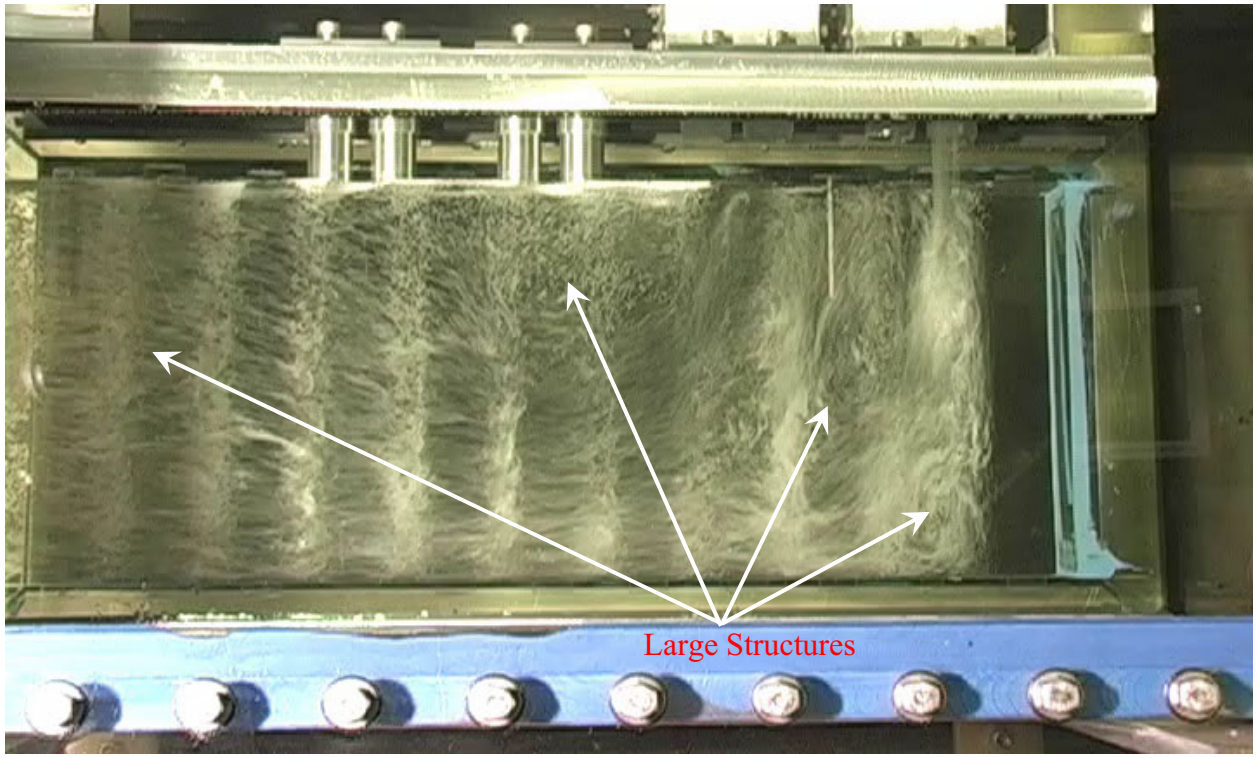

Figure 9. Flow Visualization of Four Jets Operating at ReJet ~ 4300.

check for data obtained by the PIV system. Although the movie clip represents a macroscopic view of complicated 3-dimensional flows it clearly shows four large structures that developed. The first of these structures is a vertical vortex in the bottom right corner of the model where the bottom surface of lower plenum and a model of the outer reflector wall merge. The second structure is the large vertical vortex in the vicinity of the first centerline support posts in the bottom half of the model. The third structure is a second large vertical vortex downstream of jet 4 in the upper third of the model, and the fourth structure is the contour of the outlet flow as it passes beneath the third structure (large vortex) and expands vertically upward to cover the entire exit area.

Inlet Jets

Figure 10 is a picture of four data planes taken horizontally through inlet jets 3 and 4. The flow is essentially in the downward direction (negative Vs). The flow enters the jet from the conditioning manifold (located above the top of the jet). The flow then passes through the jets and exits the jets where it enters the lower plenum. The data establish that the flow in the inlet jets is highly uniform across the jet (and reaches a velocity of about 3.2 in/sec just before entering the lower plenum. Additionally, the rather thin region of low speed flow near the jet walls indicates that the flow has developed a classic turbulent velocity profile.

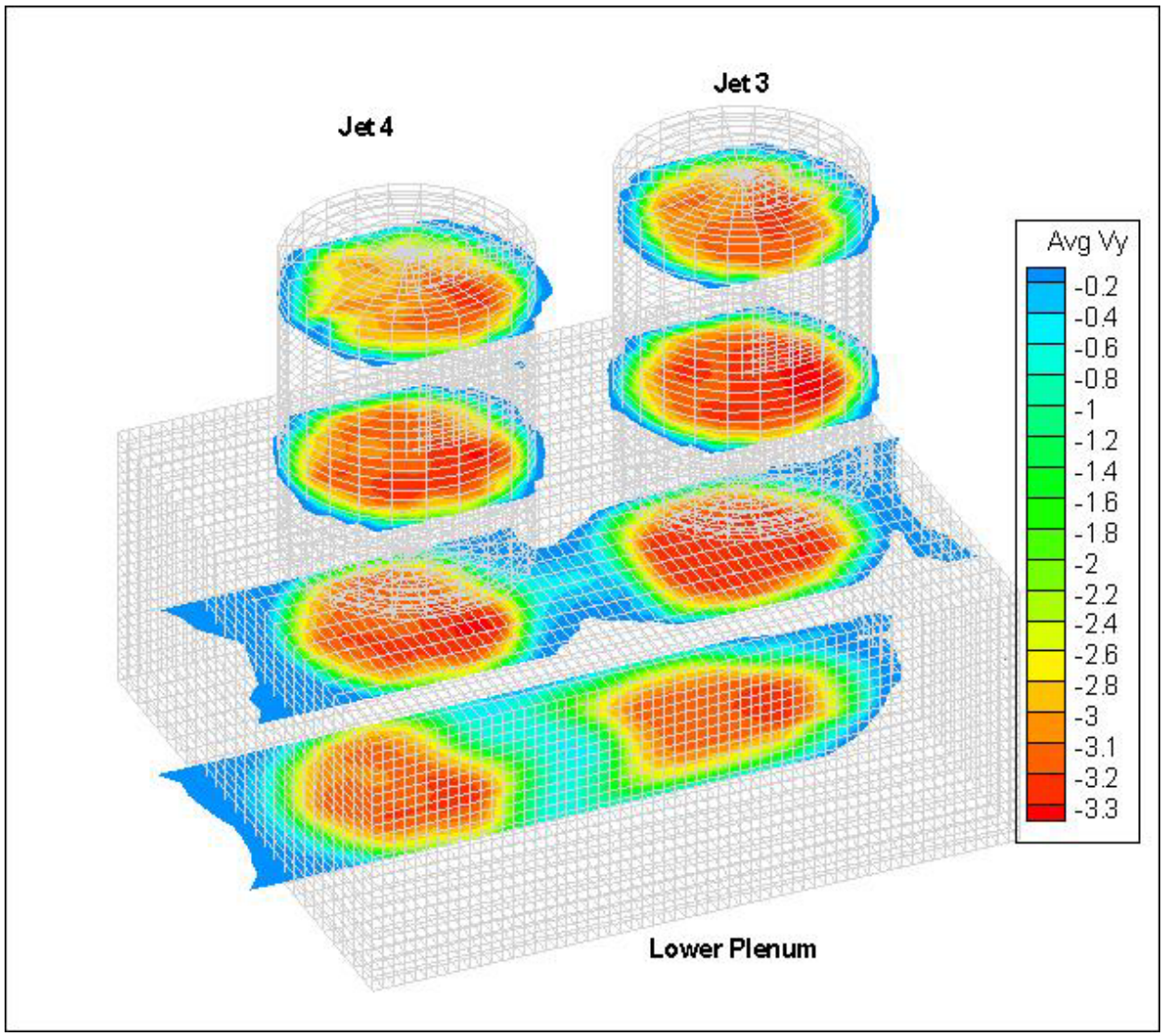

Figure 10. Data slices of vertical velocity in jets 3 and 4.

Figure 11 is a similar picture of slices that display the 3-dimensional turbulence intensity of the same flow that is shown in Figure 10. The data establish that the turbulence intensity in

this flow ranges from about 2% to 4% in the central region of the jet and increases dramatically near the wall of the jet. Similar plots describe negligible streamwise (V_x) and spanwise (V_z) velocity.

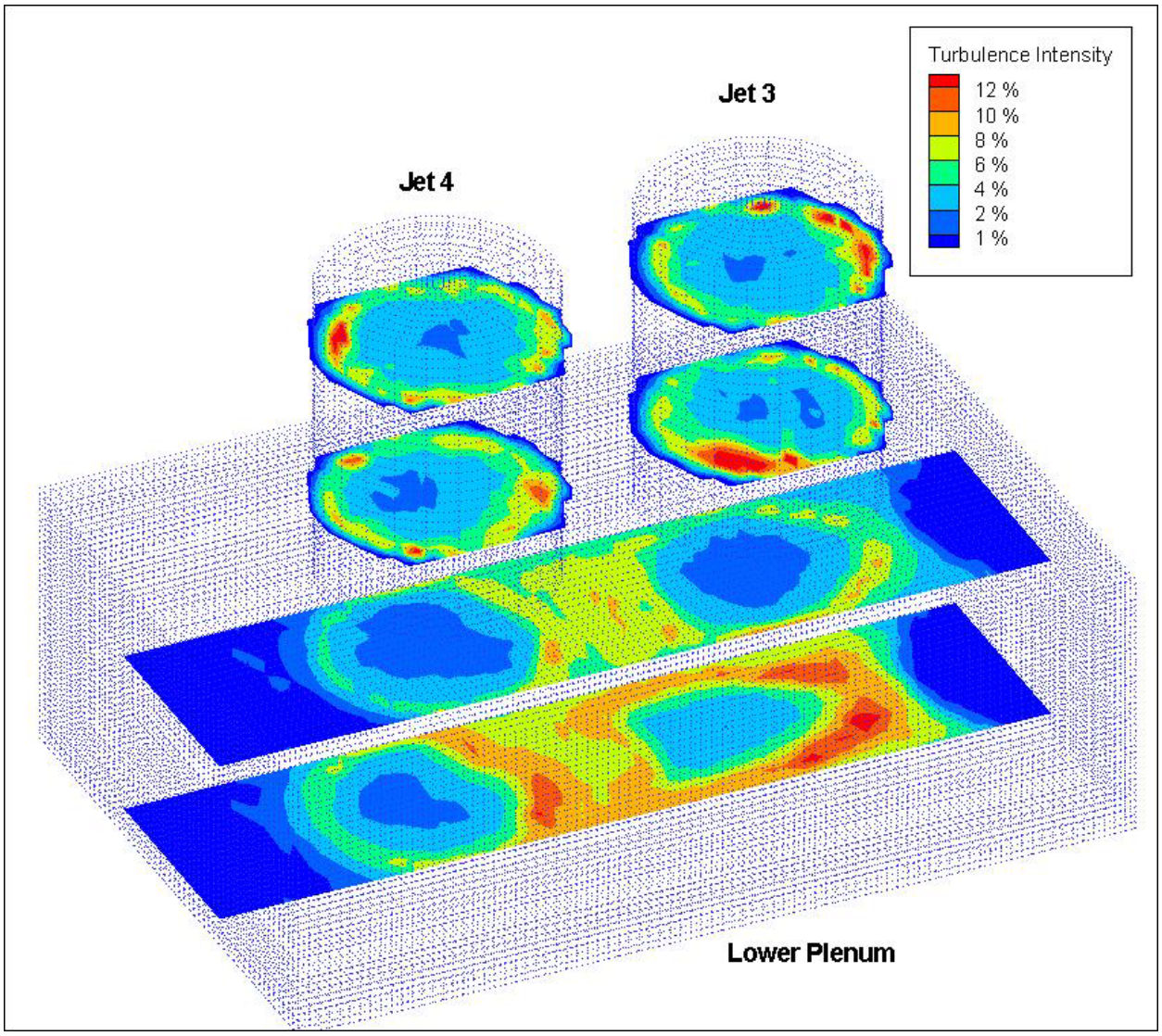

Figure 11. Data slices of 3-dimensional turbulence intensity in jets 3 and 4.

Lower Plenum

Figures 12 - 16 are a series of pictures that display a horizontal data slice through the lower plenum model 160 mm below the top surface of the plenum. Figure 12 displays the vertical velocity (V_y). The data describe flow that is essentially downward (negative V_y) near the first two support posts in the plenum but beginning to reverse and flow upward at various speeds in the remainder of the plenum. Figure 13 describes highly complicated spanwise components (V_z) of the flow. The data describe both positive and negative spanwise flow throughout the model.

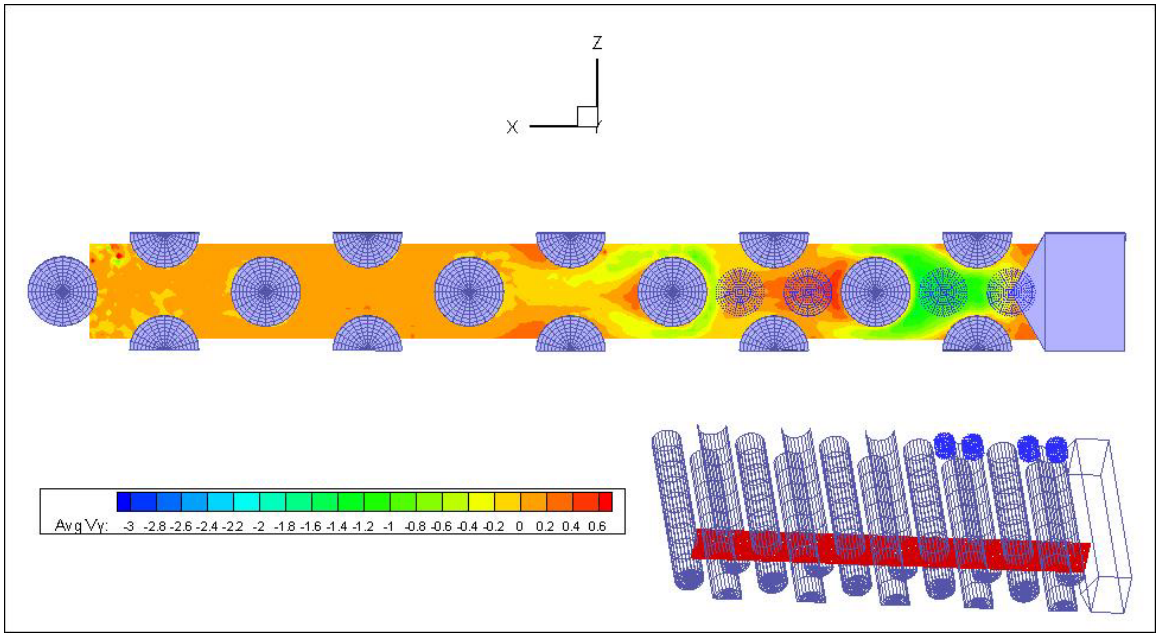

Figure 12. Data slice of the average streamwise-normal (vertical) velocity through the lower plenum 160 mm below the top surface.

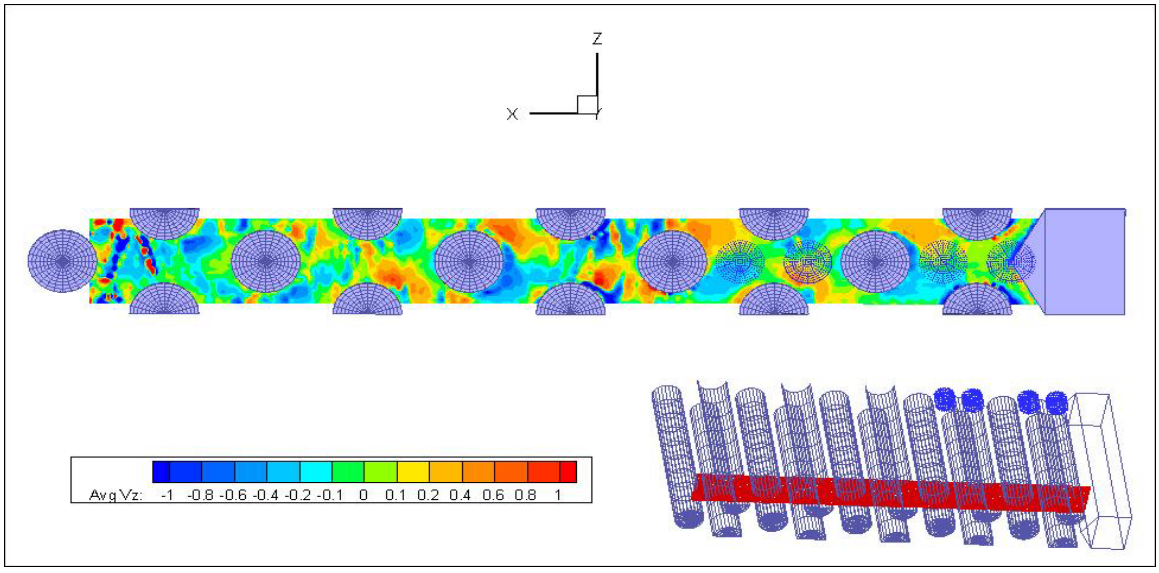

Figure 13. Data slice of the average spanwise velocity through the lower plenum 160 mm below the top surface.

Figure 14 describes a flow that is highly turbulent below both pairs of inlet jets and downstream of the post just downstream of jet 4. Additionally, decay in the turbulence intensity is evident once the flow passes the downstream of the third support post and continues toward the model exit (left end of the model). Figure 15 describes the average kinetic energy of the flow through a slice 160 mm below the top of the plenum.

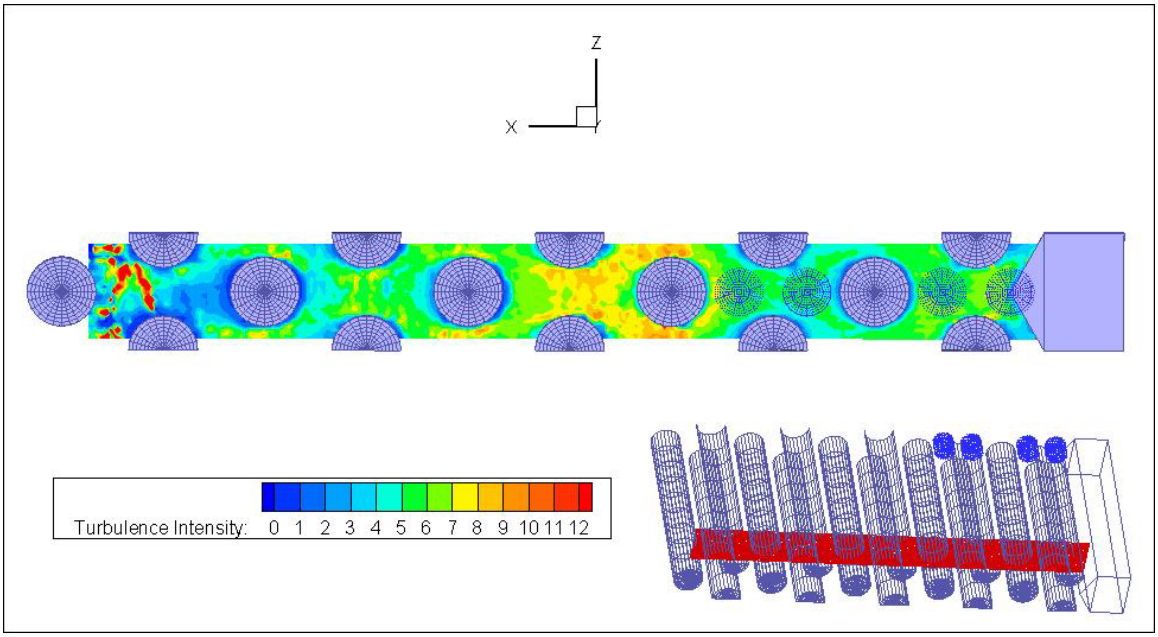

Figure 14. Data slice of the average turbulence intensity through the lower plenum 160 mm below the top surface.

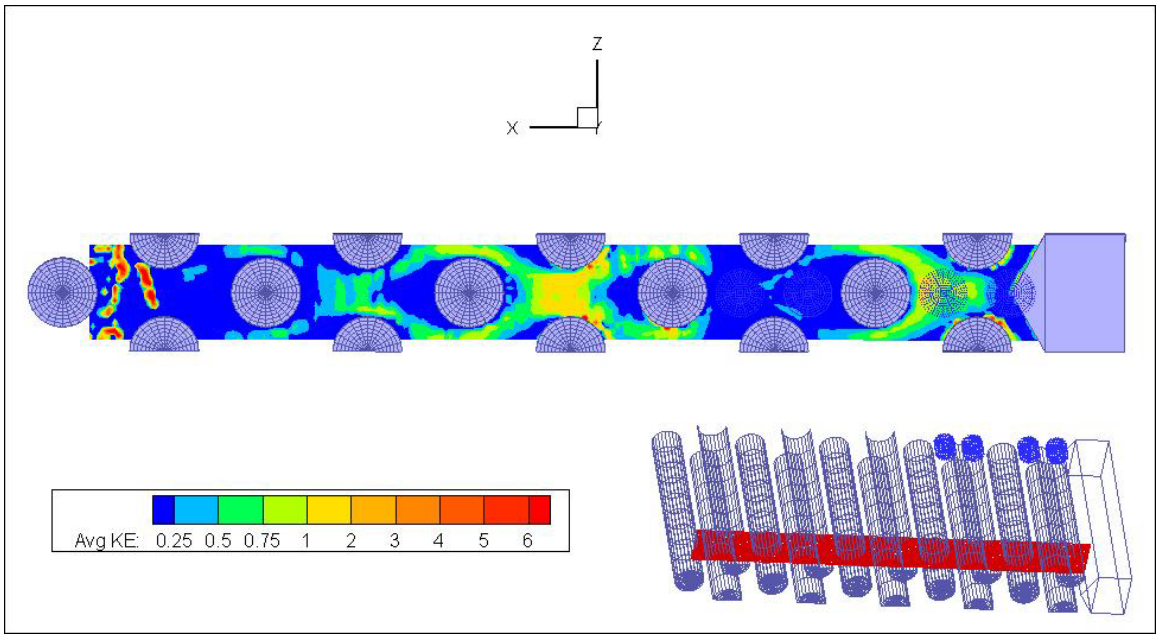

Figure 15. Data slice of the average kinetic energy of the flow through the lower plenum 160 mm below the top surface.

Figure 16 displays data slices of the streamwise (horizontal) velocity (V_x) through the lower plenum about 160 mm below the top surface of the plenum. This data describe flow that generally proceeds toward the outlet of the model (left end) but reverses around the downstream

edge of the support posts and near the half posts on the model wall. The streamwise flow is also observed to reverse near the outer wall reflector on the right side of the picture which is consistent with the observations made in the air-bubble visualization.

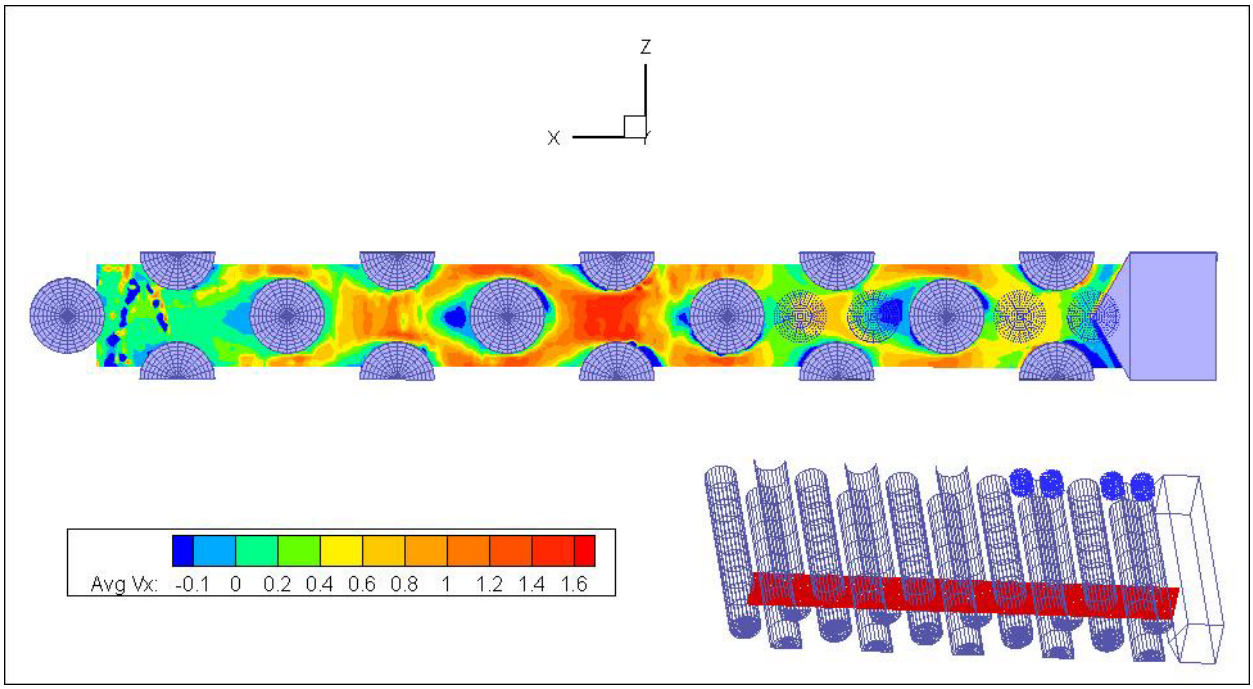

Figure 16. Data slice of the average streamwise velocity through the lower plenum 160 mm below the top surface.

Re_{Jet} 12400

A complete 3-D PIV data set of the lower plenum and inlet jets at Re_{Jet} 12400 has been collected. The data set includes the six regions of the lower plenum that were investigated with 50 mm lens and two regions to investigate the two pairs of inlet jet flows with 105 mm lens. These data were collected using 750 images for each file which requires much longer processing time. The processed data should be ready for distribution by the end of September/early October.

UNCERTAINTY ANALYSIS

The objective of uncertainty analysis relative to this experiment is to develop an understanding of the experimental uncertainties in the results. For proper benchmark databases, the experimental uncertainties of all measured quantities and their propagation into the results must be obtained quantitatively. In a complicated experiment, such as the MIR lower plenum study, some experimental uncertainties can be expected to vary significantly with position as the local velocities vary. As a partial tabulation, estimated uncertainties which are expected to be required include model geometry, measurement positions relative to the model, instantaneous

and mean velocity components and their mean statistics, transient mass flow rates, transient temperatures and pertinent instrument characteristics (e.g., laser light sheet thickness).

A detailed report of the uncertainty analysis is undergoing final review and will be available for reference in the near future.

Estimates of PIV Measuring Uncertainties

Since the basic measurement of a PIV system is an instantaneous velocity component deduced from the translation (Δx_p) of a group of particles over a time interval (Δt) so that

$$V_p = \frac{(\Delta x_p)}{\Delta t}$$

where the subscript ***p*** indicates a measurement in pixels of the recorded image, the basic per cent uncertainty in the velocity can be represented as

$$(\%Unc\, V_p) = \left[(\%\, Unc\, \Delta x_p)^2 + (\%\, Unc\, \Delta t)^2\right]^{1/2}$$

The propagation of such uncertainties into the mean statistics reported then depends on the extent to which the uncertainties are random (precision) or systematic (bias) and the manner of presentation of results. In some situations fixed uncertainties can be removed from the presentation by normalizing the quantities involved. The averaging process for determining mean statistics will reduce the resulting per cent uncertainties when they are random. Tutorial slides from LaVision provide estimates of the accuracy of vectors for calculations done with their standard FFT correlation. With twenty particles in an interrogation area of 32 x 32 pixels, bias and rms errors vary from about 0.025 to 0.1 pixels for displacements Δx of one to ten pixels. With the interrogation area of 16 x 16 pixels and 200 particles, these uncertainties fall in a range of about 0.1 to 0.2 pixels up to Δx of seven and then they explode. By employing an adaptive multipass technique first with 64 x 64 pixels and then 32 x 32 pixels, bias and RMS errors are reduced to about 0.03 pixels for up to ten pixel displacements. LaVision suggests that RMS-error is a function of the size of interrogation window, number of particles, local velocity, gradients inside the interrogation window, non-matching particles (V_i) and noise such that RMS-error (random uncertainty) is typically 0.05 to 0.1 pixels in real data.

LaVision also notes that particle image diameter of less than one pixel can cause bias during vector calculation. They recommend a particle image diameter of at least two pixels. The processing algorithm for the LaVision PIV system gives uncertainties in displacements of about 0.05 pixels for synthetic images. For images of real experiments additional factors involved include calibration, focus, displacement of particles, particle seeding, spatial gradients within each interrogation spot, image contrast, operator settings, etc. Therefore, the value of 0.05 pixels probably can be considered to be about the best possible under ideal circumstances.

For the LaVision PIV system, the random uncertainty in the timing is estimated to be about 1 nsec. For the typical pulse separation of 100 μsec (or more) used for the MIR PIV, the uncertainty would be about 0.001 (or less) per cent and therefore negligible compared to the displacement uncertainty.

To convert the basic PIV observation to actual velocities a scaling factor is employed relating the pixel dimensions to physical distance in the field of view. This quantity can suffer from both systematic (or fixed) and random uncertainties. The physical distance can be provided from a calibration device, fabrication sketches with tolerances, as-built drawings and/or independent measurements. The connection to the pixel grid is obtained via the camera view for the same location(s). In three-dimensional operation with two cameras, a LaVision calibration plate and related software are employed to relate the observed image dimensions in pixels to physical distances in the oil. From this determination a scale factor can be calculated in pixels/mm or vice versa. Currently we do not have estimates of the uncertainties involved in this process. Also, in three-dimensional operation, the laser sheet thickness may be determined from measuring a correlation peak once a self calibration procedure is completed. For the current operation the laser light sheet thickness is estimated to be 2 ± 0.2 mm.

Sample Size

Measurements of the flow field in the lower Reynolds number experiments (Re_{Jet} 4300) were made with only 170 image pairs per file. This procedure was adopted to capture the flow variations at the maximum frequency of the PIV system. This technique required that the images be stored in the LaVision PTU RAM which limited each file to 170 images. The resulting data suffered from an insufficient number of independent realizations necessary to produce reasonable mean statistics. For this reason the measurement data from the lower Reynolds number flow is considered to preliminary at best.

For the higher Reynolds number experiments (Re_{Jet} 12400), the effects of sample size for a typical set of measurements was examined using an approach comparable to that of Uzol and Camci [6]. Three thousand images of a region below a single inlet jet inlet were collected. The region below an inlet jet was selected because it offered a wide range of velocity and turbulence intensity. The variations in mean statistics were evaluated at seven locations as the number of samples was varied from 100 to 1500. Mean velocities varied from about 9 m/sec to 0.7 m/sec for these seven positions and mean-squared fluctuations varied from about 0.05 m^2/sec^2 to 4 m^2/sec^2. About ten per cent of the vectors under the inlet jets and at the bottom of the plenum in the slower region were rejected by the DaVis software while in the middle of the plenum about thirty per cent or more of the vectors were rejected The mean statistics calculated were based on the number of *valid* vectors at each point. Thus, for 1000 samples there would have been about 700 to 900 individual realizations, depending on the location.

This approach evaluates effects of random uncertainties on the mean statistics for this particular situation (view and processing). Trends were generally as observed by Uzol and Camci. Preliminary conclusions were that for this view and processing parameters about 750 images should be collected to reduce the scatter in mean velocity statistics to between 0.4 and ten per cent for velocities greater than about two m/sec.

For this study of sample size, the time interval (dt) was 120 microseconds and the scaling factor was about 9.4 pixels/mm so the estimate of random uncertainties is about 0.3 m/sec, using a displacement uncertainty of 0.3 pixels. Mean velocities varied from about nine

m/sec in the jet to 0.7 m/sec in the middle of the plenum. Corresponding instantaneous uncertainties were about three and forty per cent, respectively. For 1000 samples, these values were about 0.1 and two per cent. The former is consistent with the scatter observed in the sampling study but the latter is about an order-of-magnitude less. Approximate levels of mean-square-fluctuations were 0.05 m^2/sec^2 and 1.5 m^2/sec^2 for these two extremes (giving turbulence intensity over 100 per cent in the second case). The resulting random uncertainties are then 0.003 m^2/sec^2 and 0.02 m^2/sec^2, respectively. Both of these values are less than the scatter observed in the data processing.

The trends predicted by this uncertainty analysis are consistent with the observations but, for the most part, the expected values are less than the scatter observed. Possible explanations are that the displacement uncertainty has been underestimated, that a periodic process such as eddy shedding is affecting the results and/or some other unknown reason(s). Preliminary conclusions from the comparison were that more samples should be collected than predicted by the uncertainty analysis and the time intervals (dt) should be evaluated and adjusted for the specific conditions of each collection region.

Positioning Uncertainties

A three-directional traversing mechanism designed for use with the INL LDV was used to avoid relative motion between the test section and the optics. This traverse system supports the two digital CCD cameras and can measure model locations in conjunction with a PIV camera and its cursor. For all directional motions, platforms are moved under precise computer control to maintain alignment. Positioning is computer-controlled and determined with digital readouts with accuracy of ± 0.0001 inch or about ± 2.5 μm. The readout displays movement increments of 2 μm.

For measurements in the vertical plane of the light sheet (i.e., x and y), the origin of the model coordinate system is taken at the upstream end of the model on the vertical center plane where it intersects the top of the model flow passage (bottom of the upper quartz block). To determine locations within the image views, secondary reference positions have been established. For this purpose, holes have been bored vertically in two central quartz posts on their centerlines; pointed metal rods were installed in these holes to provide known reference points (within their fabrication tolerances). For views which do not include one of these reference positions, a reference is established at an intersection between the vertical center plane and the upstream (or downstream) face of a central post where it meets the bottom of the upper quartz block or the top of the lower block. (Since the oil temperature is adjusted to match refractive indices at 532 nm, it is possible to see quartz-oil interfaces in the camera view and at other wave lengths in the visible spectrum.)

The estimated uncertainty in absolute location of a secondary reference in model coordinates depends on the propagation of fabrication tolerances for reference post locations, reference post hole diameters, diameters of the ends of the reference posts, etc. For the current experiment, it is estimated that a point in an image may be determined to within about 0.11 mm (0.0043 in.) by using the cursor and image magnification. Thus, a relative location between two points within the same image view may be determined to about $(2)^{1/2}$ x 0.11 ≈ 0.16 mm (0.006

in). The DaVis software of LaVision also has a measuring tool that is calibrated to model dimensions during the calibration procedure. This measuring tool may be employed to determine distances between two points in a view but currently we do not have estimates of its experimental uncertainties.

During experiments the x, y and z locations of the camera traverse and the z location of the laser light sheet are recorded for every file. This information may also be employed as a check to determine where a point in an image is located relative to the model origin.

Additionally, the position of the laser light sheet is controlled by a stepping motor and linear stage with digital readout. The laser head is mounted on a linear stage that is positioned under the test section. The streamwise position of the laser head is made by hand (a non-critical position) but the spanwise position of the laser head (and laser light sheet) is controlled by the stepping motor. The linear stage and digital readout accuracy is ± 0.0002 inch or about ± 5 μm.

Seeding Particle Settling Velocity

An approach to examine the question of particle motion is in terms of settling velocity or terminal velocity due to gravity. The terminal velocity for a small particle falling through a stagnant fluid due to gravitational forces can be estimated via a force balance for steady motion,

$$\frac{dV}{dt} = 0 = \left(\frac{4}{3}\right)\pi a^3\left(\rho_p - \rho_f\right) - 6\pi\mu a\phi V.$$

The first term is the difference between the gravitational force and buoyancy while the second represents drag on the particle. The quantity ϕ is a correction factor relative to Stokes drag; it approaches unity as the particle Reynolds number approaches zero. This relation can be rearranged to yield the settling velocity as

$$V \approx \left(\frac{2\,a\,g}{9\nu}\right)\left[\left(\frac{\rho_p}{\rho_f}\right) - 1\right].$$

For our particles of about 1.7 g/cc and radii of 10 microns in our oil, this estimate gives about 0.02 mm/sec or less and $Re_p \approx 3 \times 10^{-5}$. The lowest flow velocity we might encounter is about one cm/sec. Thus the particles are expected to follow the flow adequately for the Ply.

Fluid Properties

The key fluid properties in an MIIR experiment are the fluid density, kinematic viscosity and – for optical calculations – the refractive index. These properties were measured at the University of Idaho by Orr, Thomson and Bud wig [1998] and at INL by Glenn McCreery as:

Density

$$\rho = 0.8449 - 0.0005883 \cdot T \qquad \pm 0.002 \, {}^{g}\!/_{mL} \, ;$$

Kinematic viscosity

$$\nu = 269.39^{(-0.9366)} \cdot T \qquad \pm 0.3 \, cS \, ; \text{ and}$$

Refractive index

$$n = 1.463753 - \left(3.587 \times 10^{-5}\right)\left(T - 20\right) \qquad \pm 0.0003$$

where T is measured in degrees C.

During current experiments, the oil temperature is routinely maintained at 23.3 ºC ± 0.02 ºC for the main test section (main flow) and ± 0.05 ºC for the model flow; these variations contribute to random uncertainties in measurement series. The related bias uncertainties are about 0.2%, 2% and 0.02% for the calibrations of ρ, ν and n, respectively. The random uncertainty in kinematic viscosity due to temperature fluctuations of 0.05 ºC would be 0.2%.

Geometry

As-built measurements of model components have demonstrated that the resulting dimensions are within the tolerances specified in the fabrication sketches. For the key internal dimensions these tolerances are ± 0.002 inches (0.05 mm) with the exception of the post heights which are ± 0.005 inches (0.13 mm). The diameters of the jet inlet ducts are specified as 0.870 ± 0.002 inches (22.1 ± 0.05 mm) for bias uncertainties of about 0.2%.

Flow Rates

Flow is provided to the four inlet jets from the top of the model. The total flow rate is indicated by the flow through a turbine flow meter and a Coriolis flow meter in the auxiliary temperature control system. However, the turbine flow meter is not calibrated and, in the past, has been found to be unreliable with the oil. The flow rates to the jets are measured individually with four variable area flow meters from Flowmetrics, Inc. The flow meters have a stainless steel float. The manufacturer claims that they are calibrated for our approximate operating conditions to within one-half per cent of reading, with an effective flow range of 2.5 to 60 gpm of mineral oil. This uncertainty can be considered to be a bias uncertainty. Typical minimum flow rates (for jet flows at Re_{Jet} 4300) are about sixteen gpm so the float level can be expected to be near quarter-scale or above. The principle of operation of the flow meter is that the float configuration forms a sharp-edged annular orifice with the surrounding circular tube with its differential

pressure force balancing the effective weight of the float. A force balance in terms of the orifice loss coefficient (which is a function of level) can be derived to provide a relation between the velocity through the orifice and the liquid density; the geometric quantities are fixed at a given level. This relation can be rearranged to permit measurement with a fluid of one density after calibration with a fluid of another density. The loss coefficient is relatively independent of Reynolds number except at low flow rates (low Reynolds numbers). The manufacturer indicates that for this model the viscosity immunity ceiling is 46 cp at a fluid specific gravity of 1.00 or, effectively, 14 cS. The conversion from one fluid to another will involve bias uncertainties due to uncertainties in the densities and, during experiment operation, random uncertainties from the effects of temperature variation on the density of the operating fluid. Uncertainties in reading the flow rates from the meters would be random uncertainties of about one-quarter to one-half division. The present meters have two scales. The glass tubes are scribed in millimeters from zero to the maximum of 600 mm. A separate scale provides the calibration for an oil (at 100 degrees F to give a kinematic viscosity of 14 cS) in intervals of 0.25 gpm from 1.75 to 60 gpm. Current practice is to use the calibrated scale for setting and measuring the flow rate. The specified oil density of the calibration is 0.83 g/mL, implying an uncertainty of 0.005 g/mL. This uncertainty converts to a bias uncertainty in measured flow rate of about 0.34%, a fair fraction of the one-half per cent claimed by the manufacturer. Our target oil temperature of 23.3 ºC gives an oil density of 0.8312 g/mL which is well within the range of uncertainty of the calibration density. Uncertainties in reproducing the specified flow rates of an experiment depend on the manner in which these flow rates are set. It is estimated that the flow rate settings can be repeated to within about 0.125 gpm for each jet. The lowest flow rates of the $\mathrm{Re}_{\mathrm{Jet}}$ 4300 experiments are typically 11.2 gpm (float height about 12 mm) for the first jet, which has a smaller cross section than the rest, and 16.7 gpm (about 18 mm) for the other three. Since the total volume flow rate is obtained by adding the flow rates from the individual jets operating, the absolute random uncertainty of the total is given by the absolute uncertainties of the number of jets operating as

$$\delta Q_{Total} \approx \left[N_{Jets}\right]^{1/2} \delta Q_{Jet}$$

since their random uncertainties are the same. At 11.2 gpm the bias uncertainty would be one-half per cent or about 0.06 gpm and the random uncertainty can be taken as 0.125 gpm or about one per cent. For the jets at 16.7 gpm the bias uncertainty would be about 0.08 gpm and the random uncertainty would again be 0.125 gpm. As an example, if the first and third jets were operating, the bias uncertainty of the total would be

$$\delta Q_{Total} \approx \left[(0.056)^2 + (0.084)^2\right]^{1/2} \approx 0.01\,\mathrm{gpm}$$

while for the random uncertainty it would be

$$\delta Q_{Total} \approx (2)^{1/2} \cdot 0.125 \approx 0.018\,\mathrm{gpm}$$

For this total flow rate of 27.9 gpm, the per cent uncertainties would be about 0.4 and 0.6 per cent for the bias and random uncertainties, respectively. At higher flow rates the bias uncertainties would become larger than the random ones. The per cent uncertainties in the mass flow rates $(\dot{m} = \rho Q)$ are given via the per cent uncertainties in the volume flow rates and the oil density which is given from the temperature measurements. In general, one can say

$$\frac{\delta \dot{m}}{\dot{m}} \approx \left[\left(\frac{\delta \rho}{\rho} \right)^2 + \left(\frac{\delta Q}{Q} \right)^2 \right]^{1/2}.$$

Reynolds Numbers

The jet inlet Reynolds number is defined as

$$\mathrm{Re}_{Jet} = \frac{V_b \, d_{Jet}}{\nu}$$

this can be converted to

$$\mathrm{Re}_{Jet} = \frac{4 \dot{m}_{Jet}}{\pi \, d_{Jet} \, \mu} = \frac{4 Q_{Jet}}{\pi \, d_{Jet} \, \nu}$$

so the percent uncertainty in Re_{Jet} can be estimated from the rms sum of the per cent uncertainties of these variables. For a single jet

$$\frac{\delta \mathrm{Re}_{Jet}}{\mathrm{Re}_{Jet}} \approx \left[\left(\frac{\delta Q_{Jet}}{Q_{Jet}} \right)^2 + \left(\frac{\delta d_{Jet}}{d_{Jet}} \right)^2 + \left(\frac{\delta \nu}{\nu} \right)^2 \right]^{1/2}$$

At a flow rate of 11.2 gpm, the bias uncertainty would be

$$\frac{\delta \mathrm{Re}_{Jet}}{\mathrm{Re}_{Jet}} \approx \left[(0.005)^2 + (0.0023)^2 + (0.0213)^2 \right]^{1/2} \approx 0.022 \approx 2\%$$

and the random uncertainty would be

$$\frac{\delta \mathrm{Re}_{Jet}}{\mathrm{Re}_{Jet}} \approx \left[(0.011)^2 + (0.0023)^2 \right]^{1/2} \approx 0.011 \approx 1\%$$

The bias uncertainty is dominated by the uncertainty in the calibration of viscosity (v) and is relatively independent of the other two uncertainties. The per cent random uncertainty will decrease as the flow rate increases.

SUMMARY AND CONCLUSIONS

The model design and flow facility produced satisfactory flow conditions as required by previous scaling studies and model design. As a result of the experiments described in this report

the objectives of developing benchmark databases for the assessment of CFD solutions of the momentum equations, scalar mixing and turbulence models for typical prismatic VHTR plenum geometries in the limiting case of negligible buoyancy and constant fluid properties have been met. Additionally, the data obtained from these experiments meets the requirements of a standard problem.

Preliminary measurements of velocity components have been compiled for a low-power case of Re_{Jet} ~ 4300 and detailed measurements of the flow filed for the maximum achievable flow rate in the present MIR Flow facility of Re_{Jet} ~ 12400 have also been completed. The data have been documented to identify and report uncertainty of the measurements and collected into various formats suitable for release to the CFD community and others as necessary.

Recommendations for Further Study

The work accomplished to date, which has documented flow measurements in the case of a low reactor power situation (Re_{Jet} ~ 4300) and at a relatively normal reactor power situation of (Re_{Jet} ~ 12400) with all four jets operating should be complimented with additional data to more fully characterize the flow that could be expected in a full-scale VHTR lower plenum and to provide additional data for CFD code assessment.

The data collected during the period of this report reveals the flow conditions when all four inlet jets are operating in the region of the lower plenum near the outer reflector wall away from the plenum outlet. Additional experiments should be conducted to:

- Collect data from the present model at Re_{Jet} 4300 and Re_{Jet} 12400 with only jet 1 operating (jet nearest reflector wall with partial obstruction) and also with a single pair of jets (jets 3 and 4) operating;

- Collect data with all four jets operating and with the single jet and single pair of jets identified above at an intermediate Re_{Jet} of 8000;

- Remove the model reflector wall, re-configure the model with inlet flows into jets 5 – 8 and collect data on the model with four jets operating in a crossflow at Re_{Jet} 4300, 8000 and 12400;

- Collect data with only jets 5 and 6 operating with the upstream reflector wall in place to examine the effect of the wall on jet flow between a pair of posts; and

- Conduct experiments with the laser Doppler velocimetry (LDV) system to investigate flow phenomena near the walls and post surfaces and to investigate the temporal characteristics of the flow (dominate and secondary frequencies, etc.).

ENDNOTES

[1] Lee, W. J, Wei, T. Y. C., and Schultz, R. R., et al., “Generation of a Preliminary PIRT (Phenomena Identification and Ranking Table) for Very High Temperature Gas-Cooled Reactors,” KAERI/TR-3050/2005, INL/EXT-05-00829, ANL-GenIV-066, September, 2005.

[2] Initial Measurements for Task Id of FY-O5 Work Package 10204K01 of 9 Nov 2005.

[3] McEligot, D. M. and McCreery, G. E., "Scaling Studies and Conceptual Experiment Designs for NGNP CFD Assessment," lNEEL/EXT-04-02502, 30 November 2004.

[4] Condie, K. G., McCreery, G. E., McIlroy, H. M. Jr., and McEligot, D. M., "Development of an Experiment for Measuring Flow Phenomena Occurring in a Lower Plenum for VHTR CFD Assessment," LNL/EXT-05-00603, 21 September 2005.

[5] Stoots, C., Becker, S., Condie, K., Durst, F., and McEligot, D., 2001, "A Large-Scale Matched Index of Refraction Flow Facility for LDA Studies Around Complex Geometries," Exp. in Fluids, **30,** pp. 391-394.

[6] Uzol, C. and Camci, C., 2001, "The Effect of Sample Size, Turbulence Intensity and Velocity Field on the Experimental Accuracy of Ensemble Averaged PIV Measurements," 4th International Symposium on PIV, Göttingen, Ger, Sep 17-19.